LEARNING PEG-IN-HOLE ACTIONS WITH FLEXIBLE OBJECTS

Leon Bodenhagen[1], Andreas R. Fugl[1,2], Morten Willatzen[2], Henrik G. Petersen[1] and Norbert Krüger[1]

[1]*Maersk McKinney Moller Institute, University of Southern Denmark, Campusvej 55, 5230 Odense, Denmark*

[2]*Mads Clausen Institute, University of Southern Denmark, Alsion 2, 6400 Sønderborg, Denmark*

Keywords: Peg-in-Hole, Flexible objects, Action learning.

Abstract: This paper presents a method for learning Peg-In-Hole actions with flexible objects. To learn the actions we parametrize the entire trajectory by a single point and use Kernel Density Estimation to reflect the different variations of the action and the object characteristics. The object is characterized by its elastic behaviour rather than geometric properties. Thereby an action learned for one object can be transferred to a new object that behaves similarly although it might have different elastic properties, dimensions and geometries. To bootstrap the learning mechanism, the system performs simulated actions and utilizes the detailed information obtained from the simulation environment. Subsequently Peg-In-Hole actions are tested successfully on the real life setup.

1 INTRODUCTION

Humans can perform a huge variety of different and apparently simple tasks, but often such tasks are difficult for robots to perform. The Peg-In-Hole problem is one of these tasks and has been studied in numerous works with different perspectives and objectives, often as an example of an assembly task.

One of the aspects investigated is for instance, in addition to the insertion of the peg, the exact alignment of the peg with the hole (Bruyninckx et al., 1995). Assuming that the shape of both the (rigid) peg and the hole is known, the contact forces during the operation can be predicted (Meitinger and Pfeiffer, 1996) and used to optimize the action. More recent approaches often focus on sub-aspects of the classic Peg-In-Hole task. Elastic contacts have for instance been utilized in (Xia et al., 2006) to avoid wedging.

However, to our knowledge only little work has been done with flexible objects in the context of Peg-In-Hole operations or assembly tasks in general (see also (Jiménez, 2011)). In (Villarreal and Asada, 1991) the concept of flexible objects has been used to model finite collision forces between the object and the rim of the hole and thereby aid the motion planning by providing it a “buffer“, but in general the shape is considered to stay roughly constant. Path planning with simple, flexible 3D objects like tubes that change their shape during operation are done by (Anshelevich et al., 2000). They model the objects by mass-spring models and perform a random search for the path with the minimal energy. Such an approach is however not feasible when a variety of non-trivial 3D shapes is considered.

In general it is intractable to model and plan the entire action when the deformation of the object has to be considered during the action, therefore this paper investigates an approach that avoids heavy online calculations. Furthermore a classic force-torque sensor can hardly be utilized as any contact will, in addition to measurable forces, cause a deformation of the object - hence standard approaches used for Peg-In-Hole actions with rigid objects cannot be applied.

In this paper we propose a system that learns how to perform the Peg-In-Hole operation with flexible objects (see Figure 1). The learning mechanism has only little prior knowledge about the object; instead the learning utilizes a physical modelling from the elastic properties of the object. The elastic behaviour is derived from calculating the deformation of the bottom surface in the object. By this surface the object is implicitly deformed in the learning stage. This allow us to handle non-trivial 3D shapes in a low-dimensional way. Further a learned action can be transferred to a similar but not necessarily identical object. This leads to a system that can perform in real time as the demand for servoing or online modelling becomes minimized, assuming that most objects in e.g. a production scenario indeed are similar.

The overall system that forms the context for the

Bodenhagen L., R. Fugl A., Willatzen M., G. Petersen H. and Krüger N..
LEARNING PEG-IN-HOLE ACTIONS WITH FLEXIBLE OBJECTS.
DOI: 10.5220/0003882806240631
In *Proceedings of the 4th International Conference on Agents and Artificial Intelligence* (SSIR-2012), pages 624-631
ISBN: 978-989-8425-95-9

action learning is outlined in section 2 and the applied methodology is described in section 3. Section 4 summarizes the experiments that have been done in order to investigate the usability of the suggested approach.

2 SYSTEM SETUP

The overall system, presented in more detail in (Jordt et al., 2011), corresponds to a short production line: Objects are transported by a conveyor belt, a 3D scan of the travelling object provides a 3D triangular mesh of the object. Assuming that the material properties are known, the elastic behaviour of the object is modelled. At the end of the conveyor this knowledge is used to grasp the object. Subsequently an additional action can be performed. The Peg-In-Hole operation is investigated in this paper as it has been considered to be characteristic for many tasks where some sort of object is inserted into a machine in order to be processed.

This paper (in contrast to (Jordt et al., 2011)) focuses primarily on the modelling of deformations as well as the learning of Peg-In-Hole actions. The robot arm with an 1-degree of freedom gripper attached is shown on Figure 1 with a close-up of a Peg-In-Hole operation.

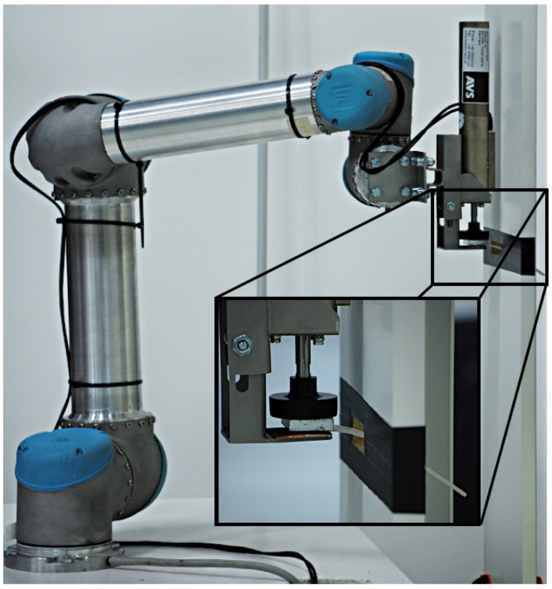

Figure 1: The physical setup used for the experiments.

3 METHODS

In the following a detailed overview of the components which this papers focuses on is given. The modelling of the deformations of objects is described in section 3.1, in section 3.2 the physical modelling is condensed into a feature vector and the formalization and learning of actions is defined in section 3.3.

3.1 Deformation Modelling

Deformation modelling in the context of Peg-In-Hole operations, is concerned with modelling the flexible objects in the scene and solving for their behaviour. We restrict the problem to the situation of the peg being substantially more flexible than other objects in the scene. Thus the boundary of the plate, defining the hole for insertion is assumed to be a rigid body, as are the jaws of the robot gripper grasping the peg.

For the flexible peg we want to determine the mechanical response, i.e. how do material points in the peg change as a function of time and external influences (modelled as forces). We assume the elastic parameters such as stiffness and mass density to be available with reasonable accuracy.

In the following, the approach to model deformation for the purpose of learning Peg-In-Hole actions will be outlined.

3.1.1 Deformation Description

Let x be a material point in the undeformed object. The object deforms and the new position of the point after deformations are added is x'. The *displacement vector* for some point is thus $u = x' - x$, or in component form:

$$u_i = x'_i - x_i \tag{1}$$

where $i = 1,2,3$ refers to the x,y,z components. The displacement vector is a dense and very general description as it explicitly provides the deformation of every material point in the flexible object. However directly using the deformation vector of material points for the parametrization of general 3D objects becomes prohibitively expensive. For the purpose of reducing the time required for sampling when learning Peg-In-Hole actions with flexible objects, it is crucial to have a sparse but still accurate representation of a deformed surface.

(Samareh et al., 1999) reviewed several shape parametrization techniques, including discrete, polynomial and spline representations. Their goal was to investigate the applicability of the techniques to describe aircraft airfoils with the minimum amount of parameters. This is important for the purpose of automatic optimization, where the shape of the wing is deformed in small increments to find the best possible aerodynamic design. In this process a large parameters space must be searched, and thus having a small amount of parameters is crucial for the feasibility of the approach.

The parametrization by the discrete approach corresponds to sampling the displacement vector at regular intervals at the boundary. It is the most straightforward method, and can approximate any shape. However as (Samareh et al., 1999) points out, this degree of freedom is rarely useful due to the inherent smoothness of many objects. For instance smooth, curving features will require many discrete points and accordingly the number of parameters can increase to unacceptable sizes.

Parametrization by polynomia and splines on the other hand exploits the smoothness of the original shape. For smooth shapes they will reduce the number of parameters considerably. The non-uniform rational B-spline, NURBS (Piegl and Tiller, 1997), is best suited for handling a large set of shapes, including analytical shapes such as cylinders, cones and scanned unstructured 3D data (Samareh et al., 1999; Bardinet et al., 1995).

As demonstrated by (Jordt et al., 2011) a realtime tracking of a detailed 3D mesh, using depth and colour video from a Kinect camera, can be coupled to a low-dimensional NURBS surface, see Figure 2.

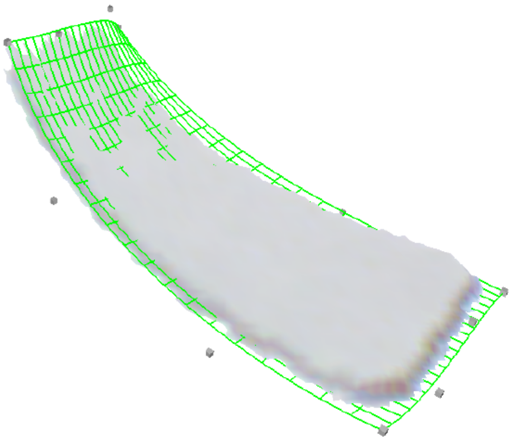

Figure 2: A scanned 3D mesh of an object and its associated NURBS surface (Figure courtesy of (Jordt et al., 2011), with kind permission by the authors).

Similarly we decouple the geometry from the deformation. Only the deformation of the control points in the NURBS surface is used as a a parameter in the learning stage.

The deformation modelling is thus reduced to the problem of finding the deformation for the control points of the NURBS surface. When at some point the whole surface deformed geometry is needed (for instance for collision detection), it is derived from the deformed control points. Having a deformation that models to the NURBS surface also enables easier coupling to the NURBS based deformation tracking.

3.1.2 Choice of Model

The Bernoulli-Euler (BE) beam theory has since its development in the 18th century, been a core element in structural engineering. Its' formulation and parameters are readily understandable, and many problems have analytical solutions. It is a simple model however, as it only accounts for the bending moment and lateral displacement of the beam.

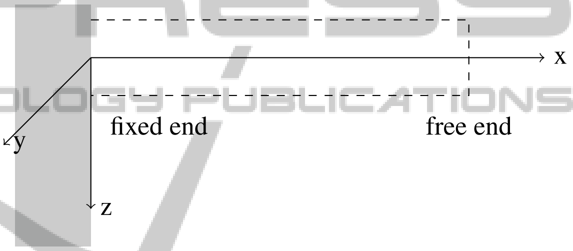

Figure 3: A cantilevered beam.

Several additional models have been developed during the years to improve on the BE model. Most noteworthy of these is the Timoshenko model (Timoshenko, 1921), which takes into the account both rotation inertia and shear deformation.

To account for the additional effects, the Timoshenko model adds a dependent variable to account for the angular displacement and a parameter known as the shape factor. The shape factor is a function of Poisson's ratio for the material, the wave frequency and the shape of the cross section. For the static case, the shape of the cross section is the most dominant effect on the shape factor[1].

The slenderness ratio is the ratio of the beam length to the radius of gyration, calculated as $L/\sqrt{I/A}$. It characterizes the magnitude of different forces involved in the beam equations. In the work of (Seon M. Han, 1999) they recommend the use of the simple BE model for large slenderness ratios ($s > 100$), and the Timoshenko model for smaller ratios where second order effects of rotation and shear become important.

[1] Poisson's ratio varies for normal materials only between 0 and 0.5 (Landau et al., 1986).

For our present experiments, we target moderately slender objects ($100 < s < 150$). Accordingly we use the BE beam theory.

3.1.3 Bernoulli-Euler Beam Theory

The governing equation for the dynamic BE beam can be formulated as a partial differential equation in the deflection w of the beam

$$\frac{\partial^2}{\partial x^2}\left(EI\frac{\partial^2 w}{\partial x^2}\right) = -\mu\frac{\partial^2 w}{\partial t^2} + q \qquad (2)$$

where $w(x,t)$ is the deflection as a function of position x on the beam and time t. E is Young's modulus, I is the second moment of inertia and q the is body load.

Young's modulus, E is a material dependent parameter and represents the stiffness of the material. It may be either measured or derived from tabulated data. For homogeneous materials it is a constant.

The *second moment of inertia*, I is a geometry dependent parameter, quantifying resistance to bending at a given cross section. It is defined as $I = \int_A z^2 dA$, where z is the height of the cross section, being perpendicular to the bending. For a geometry that has a constant cross section (e.g. a simple beam) it is a constant. For the special case of a rectangular cross section with height h and width b, I is equal to $bh^3/12$. This suggests a strong dependence of the thickness of such a beam, to the resulting deformation, i.e. varying the thickness will give the strongest resulting change.

The *body load*, q represents an external force acting upon the beam. It is defined as a force per unit length. Point forces may be modelled with the use of the Dirac delta function.

For the static case of a homogeneous beam with constant cross section, Equation 2 reduces to the ordinary differential equation (ODE)

$$EI\frac{d^4 w}{dx^4} = q(x) \qquad (3)$$

where $w(x)$ is the deflection now only as a function of position, and E and I are both constants.

The static beam equation, Equation 3 is a fourth-order ODE. In order to find a unique solution for the deformation profile $w(x)$, four boundary conditions must be prescribed. Assuming that the gripper is placed such that the left end of the object at $x = 0$ is fixed in space (both deflection and slope equal to zero) we have the boundary conditions for the clamped end

$$w|_{x=0} = 0 \quad ; \quad \left.\frac{\partial w}{\partial x}\right|_{x=0} = 0 \qquad (4)$$

For the other end of the object at $x = L$, we prescribe the boundary conditions (both the bending moment and the shear force in the beam is zero) corresponding to that this part of the object is free to move

$$\left.\frac{\partial^2 w}{\partial x^2}\right|_{x=L} = 0 \quad ; \quad \left.\frac{\partial^3 w}{\partial x^3}\right|_{x=L} = 0 \qquad (5)$$

The ODE Equation 3 together with the boundary conditions Equation 4 and Equation 5 form a boundary value problem. The solution gives the deflection of a fixed-free/cantilevered beam, as depicted on Figure 3.

This boundary value problem, along with the restriction that the load is uniformly distributed i.e. $q(x) = constant$, has the analytical solution to the deflection $w(x)$ of the beam

$$w(x) = \frac{qx^2(6L^2 - 4Lx + x^2)}{24EI} \qquad (6)$$

3.2 Object Description

One aim of the action learning is to be able to apply an action learned with one object to another object that behaves similarly. The behaviour of an object is considered to be defined by the deformation that occurs when a specific grasp is applied and the object is affected by gravity - these deformations can be modelled as outlined in section 3.1.

In the following the condensation of the high-dimensional information that is intrinsic to the deformation modelling into a feature vector of lower dimensionality is described. Ideally two different objects, e.g. with different shapes, maps to the same feature vector if they behave identically, such that the same action can be applied.

In order to achieve a feature-vector that is comparable across objects, the NURBS surfaces describing the undeformed object $S_u(u,v)$ and the object in a horizontal orientation, affected by gravity $S_d(u,v)$. The length of the objects is normalized.

The difference between the two surfaces describes how much the object has deformed at the individual locations:

$$\hat{S}(u,v) = S_u(u,v) - S_d(u,v) \qquad (7)$$

Based on a regular grid g of size $I \times J$, the deformations are obtained at a set of discrete locations and for a feature vector f:

$$f = \left[\|\hat{S}(g_{00})\|, ..., \|\hat{S}(g_{ij})\|, ..., \|\hat{S}(g_{IJ})\|\right] \qquad (8)$$

where g_{ij} refers to the a point of the grid at the position (i,j). An simplified example for the calculation of f is shown in Figure 4. It correspond to a deflecting beam where the deflections can be described by a NURBS curve instead of an entire surface.

3.3 Action Learning

The exact 6D trajectory of a Peg-In-Hole operation depends both on the elastic behaviour of the object, the grasp applied to the object and the shape of the object. However, although the 6D trajectory for instance varies with the size of the object, it might still share similarities with other Peg-In-Hole actions. The parametrization of the action aims to reduce the complexity of the learning problem and eases the transfer of a learned action from one object to another as the object does not need to be identical, but only to share certain properties. The following sections cover the parametrization of Peg-In-Hole actions as well as the structure and strategy for learning them.

3.3.1 Action Parametrization

The Peg-In-Hole action is defined by a trajectory which the robot executes. The endpoint P_1 is known as it is directly in front of the hole. The startpoint P_0 is obtained online utilizing the deformation prediction and ensures that the end of the object is horizontal and in front of the hole (see Figure 5). The trajectory from the start to the endpoint is considered to be approximated by a curve defined by two-dimensional translations and one-dimensional rotations. The points P_0 and P_1 are therefore both points in $\mathbb{R}^2 \times SO(2)$.

The curve $P(t)$ is defined using a rational Bézier-curve (Piegl and Tiller, 1997) based on three control points: the start and endpoint as well as one additional controlpoint which will be obtained by learning:

$$P(t) = P_0 + B(t)(P_1 - P_0) \text{ for } t \in [0;1] \qquad (9)$$

with

$$B(t) = \frac{\sum_{i=0}^{n} b_{i,n}(t) P_i w_i}{\sum_{i=0}^{n} b_{i,n}(t) w_i} \qquad (10)$$

where $b_{i,n}(t)$ is the Bernstein polynomial with $n = 2$ and P_i refers to the i'th controlpoint for the curve:

$$P_i \in \{\mathbf{0}, cp, \mathbf{1}\} \qquad (11)$$

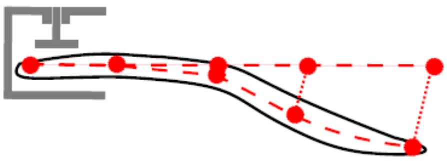

Figure 4: Illustration of the differences between the undeformed mesh (straight dashed line) and the deformed mesh (bent dashed line) used for the feature vector in a 2D case. The resulting feature vector will be 5-dimensional.

The weights are fixed, $\mathbf{w} = [1,2,1]$, which ensures that the second control point, cp, has an increased impact. Thereby also motions that lead to a significant overshoot can be learned.

Note that the control points do not depend on the scale of the motion or the object (see Equation 9). Therefore a learned control point will lead to meaningful trajectories for any object, although it is not guaranteed that the performed action will be successful.

3.3.2 Action Learning Framework

The set of potentially successful Peg-In-Hole actions is modelled using Kernel Density Estimation (Silverman, 1986). Every time a control point that leads to a successful action has been obtained, it is added to the density d. However, contrary to the situation in (Detry et al., 2011) where grasp affordances are learned for a specific object, we cannot assume the objects to be identical. Therefore a kernel, $\mathbf{K}_{\mu,\sigma}(cp,f)$, which is a compound of two kernels is used: one reflecting the Peg-In-Hole action as such, the other reflecting the object features specified in section 3.2.

$$\mathbf{K}_{\mu,\sigma}(cp,f) = \mathbf{N}^{PiH}_{\mu_p,\sigma_p}(cp)\mathbf{N}^{Object}_{\mu_o,\sigma_o}(f) \qquad (12)$$

where $\mathbf{N}^{PiH}$ and $\mathbf{N}^{Object}$ are isotropic multivariate Gaussian kernels located at the mean positions μ_p resp. μ_o and with bandwidth of σ_p resp. σ_o. The density is given by a weighted sum of the m kernels:

$$d(cp,f) = \sum_{i=0}^{m} w_i \mathbf{K}_{\mu_i,\sigma}(cp,f) \qquad (13)$$

where the weights w_i ensure that the density integrates to one, hence $\sum_i^m w_i = 1$.

During the learning every controlpoint that leads to a successful action will contribute to the density

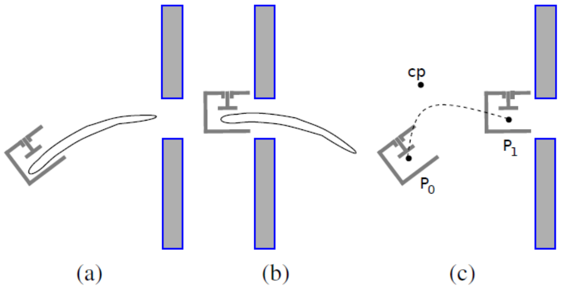

Figure 5: Illustration of (a) starting configuration P_0 and (b) target configuration P_1 for the Peg-In-Hole action. (c) shows a projection of the 3D trajectory based on P_0, P_1 and the controlpoint cp.

with one particle. Assuming that an action is either successful or not, all particles of the density have equal weights. Given an uniformly sampled search space, the value of the density at a given point will be proportional to the likelihood of the corresponding action for being successful.

Here, we choose the points for the feature vector f as those illustrated in Figure 4. It should be noticed that the point P_0 is scaled with respect to object length (see Figure 4). Thus, two objects with different lengths having the same feature vector then have equivalent shapes and may be handled in the same way except for choosing the appropriate length scaled P_0. Thus, the parameters cp and f covers a given control point and shape for all object lengths.

Assume now that we wish to solve a Peg In Hole action for a hitherto unstudied object. The deflection model is then used to compute the feature vector f_O. Then the control point with the highest probability for success can be obtained by searching for the maximum of the density $d(cp, f_O)$.

3.3.3 Action Learning Strategy

The system is not provided with any prior knowledge to bootstrap the learning strategy. Therefore a 2-step learning mechanism has been considered. First, an exhaustive search on the controlpoints is performed in a simulated environment. As the controlpoints are 3-dimensional it is feasible to explore the space with a reasonable resolution. The outcome of the simulated experiments leads to a density as defined in Equation 13. Examples for the clouds of particles are shown in Figure 7. Finally, the density achieved by simulation can be sampled and evaluated on the real-world setup, leading to a new density.

Utilizing a simulator does not only allow the evaluation of large set of experiments, it also provides a detailed feedback about the performed action. The outcome of an experiment is therefore not only a binary, namely success or failure, but also the minimal clearance c between the object and rim of the hole that is experienced during the individual experiment. A bigger clearance implies that the action is more robust to external disturbances and modelling errors. This fact is reflected by the weights:

$$w_{ij} = \frac{1}{N} \frac{c_{ij}}{\sum_{j=0}^{M} c_{ij}} \tag{14}$$

where c_{ij} is the minimal clearance of the j'th out of M successful experiments with the i'th object, given N objects in total. Thereby the maximum of the density does not only reflect the success likelihood, based on the statistics of the samples, but directly corresponds to the action that is expected to be the most robust in the given situation.

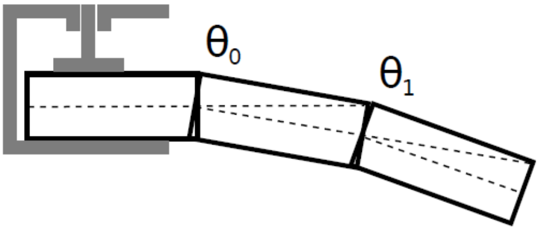

Figure 6: Approximation of a flexible object using a rigid device. Self-collisions within the simplified object model are ignored.

4 EXPERIMENTS

In the following the simulated experiments used to bootstrap the learning are described in section 4.1. Experiments on the real setup are described in section 4.2.

The test specimens are cuboid pieces of silicone rubber, cut from a sheet of 2.0 mm thickness, into pieces of 15 mm width. The density of the silicone sheet as given by the manufacturer is 1.15 g/cm^3 and the shore A hardness is 60 ± 5 (which corresponds to a Young's modulus of approximately 3.6 MPa).

4.1 Simulated Experiments

For the simulation, based on a simulation environment from (Ellekilde and Jørgensen, 2010), a flexible, cuboid object is approximated by a rigid device consisting of a set of consecutive boxes as illustrated in Figure 6. This approximation allows for efficient collision detections as well as clearance calculations - the precision can be controlled easily by adjusting the number of joints in the device. The angles of the joints connecting the boxes are obtained from the object deformation modelling which takes the orientation of the grasped object with respect to gravity into account.

Table 1: Overview over the different outcomes experienced in the simulator.

	Minimal clearance [mm]			
Object	collision	0 - 2	2 - 4	4 <
80 mm long	6899	258	288	555
60 mm long	4711	416	524	2349
40 mm long	3418	678	1267	2637

Simulations have been done for three different objects, testing Peg-In-Hole actions for each object with 8000 controlpoints. The outcomes of the experiments (summarized in Table 1) indicate that it is easier to insert short objects rather than long ones: a higher proportion of all actions succeeded and the average minimal clearance of the succeeding actions is larger. This has been expected as long objects lead to large deflections and can thus not be inserted by a close to straight-line motion in contrast to short objects.

All controlpoints learned for the short resp. long object are shown in Figure 7. In both cases the solutions form a close to convex area which indicates that the complete density can be approximated with a sparse density consisting of fewer particles, but with larger bandwidths. As the costs of the search for a maximum within the density depend on the number particles that need to be evaluated, densities based on fewer particles ease the implementation of a real-time system.

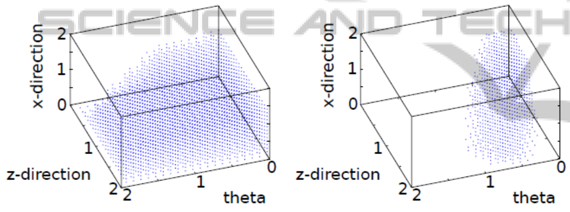

(a) 40 mm

(b) 80 mm

Figure 7: Illustration of the 3D point clouds of the controlpoints that lead to successful actions for the (a) 40 mm long object and (b) the 80 mm long object.

4.2 Real Experiments

In the following the validity of the modelled deflections as well as the learned Peg-In-Hole actions are assessed by real-world experiments.

4.2.1 Deformation Validation

To validate the modelling, the maximum deformation of each test object have been measured in a separate experimental setup.

For the test objects of $80, 60$ and 40 mm, the mean values for the deformations are respectively 29.25, 10.25 and 2.25 mm. Using the tabulated shore A hardness of 60 for the silicone rubber (corresponding Young's modulus 3.6 MPa), the deformation is overestimated. This trend is clear for the larger deformations of the piece 80 mm in length. Using an extrema of the hardness, shore A 65 (Young's modulus 4.4 MPa) the maximum calculated deflection of the piece reduces to 28.3 mm, which is closer to the observed mean of 29.25 mm.

Table 2: The maximum deflection of the respective test objects. The last column shows the deformation as calculated by the modelling, assuming a shore A hardness of 60. For each object, 4 different orientations have been independently measured.

	Measured max. deflection [mm]				
Object	O1	O2	O3	O4	Sim.
80 mm	29	28	30	30	33.5
60 mm	10	10	10	11	10.5
40 mm	2	2	3	2	2.5

4.2.2 Peg-in-Hole Actions

Based on the results of the simulated experiments, Peg-In-Hole actions with the simulated objects have been evaluated on the real setup. The controlpoints have been obtained by searching the density obtained by simulation for a maximum. The resulting actions have been observed to be successful, the last step of the insertion of the longest object is shown on Figure 1. However manual measurements of the minimal clearance have been done in order to investigate the robustness of the learned actions. Especially for the longest object, the clearance has been observed to be approximately 1 mm (for the 80 mm long object) which is lower than expected according to results in Table 1.

A potential reason for smaller clearance might be caused by alignment errors between the grasped object and the hole as even small errors seam to have a significant effect. Further the most significant difference between measured and expected clearance has occurred for the 80 mm long object, which might be correlated with the fact that the deflection modelling for this object had the bigger error than the others (see Table 2).

5 FUTURE WORK

The overall system discussed so far is, as no sensor input is used to correct for modelling errors, an open-loop system. However, when the complete scenario is considered where an object becomes scanned, modelled, grasped and inserted multiple error sources arise. If the object-relative location of the grasp is significantly different than expected, this would have an impact on the modelling and might cause the Peg-In-Hole action to fail.

To counteract potential errors an additional Kinect-camera is introduced, enabling the system to supervise the Peg-In-Hole operation. We foresee that the additional feedback can be used to:

- Improve the deflection modelling over time.
- Correct for inaccuracies during the grasping.
- Correct the starting position of the Peg-In-Hole action.

6 DISCUSSION

In this paper we presented a system to perform Peg-In-Hole action with flexible objects. The system utilizes a physical modelling of the elastic behaviour of the objects and an action learning mechanism based on kernel density estimation. Objects are identified by a distinctive feature vector that enables the system to recognize objects with similar behaviours as known objects. Thereby previously learned actions can be applied to new objects, with similarly behaviour as known ones. This enables the system to perform in real time as the demand for time consuming modelling operations is minimized.

ACKNOWLEDGEMENTS

This work was co-financed by the INTERREG 4 program Syddanmark-Schleswig-K.E.R.N. by EU funds from the European Regional Development Fund. The presented work has also received funding from the EU Seventh Framework Programme under grant agreement no. 270273, Xperience.

REFERENCES

Anshelevich, E., Owens, S., Lamiraux, F., and Kavraki, L. E. (2000). Deformable volumes in path planning applications. In *IEEE International Conference on Robotics and Automation*.

Bardinet, E., Cohen, L. D., and Ayache, N. (1995). A parametric deformable model to fit unstructured 3d data.

Bruyninckx, H., Dutré, S., and Schutter, J. D. (1995). Peg-on-hole: A model based solution to peg and hole alignment. In *International Conference on Robotics and Automation*.

Detry, R., Kraft, D., Kroemer, O., Bodenhagen, L., Peters, J., Krüger, N., and Piater, J. (2011). Learning grasp affordance densities. *Paladyn Journal of Behavioral Robotics*, 2:1–17.

Ellekilde, L.-P. and Jørgensen, J. A. (2010). RobWork: A Flexible Toolbox for Robotics Research and Education. In *International Symposium on Robotics*,

Jiménez, P. (2011). Survey on model-based manipulation planning of deformable objects. *Robotics and Computer-Integrated Manufacturing*, In Press.

Jordt, A., Fugl, A. R., Bodenhagen, L., Willatzen, M., Koch, R., Petersen, H. G., Andersen, K. A., Olsen, M. M., and Krüger, N. (2011). An outline for an intelligent system performing peg-in-hole actions with flexible objects. In *The International Conference on Intelligent Robotics and Applications (Accepted)*.

Landau, L. D., Pitaevskii, L. P., Lifshitz, E. M., and Kosevich, A. M. (1986). *Theory of Elasticity*. Butterworth-Heinemann.

Meitinger, T. and Pfeiffer, F. (1996). The spatial peg-in-hole problem. In *Proceedings of the Second World Automation Congress*, Montpellier, France.

Piegl, L. and Tiller, W. (1997). *The NURBS book*. Springer-Verlag New York, Inc., New York, NY, USA, 2. edition.

Samareh, J. A., Samareh, J. A., and Polynomial, B. B. (1999). A survey of shape parameterization techniques.

Seon M. Han, Heym Benaroya, T. W. (1999). Dynamics of transversely vibrating beams using four engineering theories. *Journal of Sound and Vibration*, 225:935–988.

Silverman, B. W. (1986). *Density Estimation for Statistics and Data Analysis*. Chapman and Hall/CRC.

Timoshenko, S. P. (1921). On the correction for shear of the differential equation for transverse vibrations of prismatic bars. *Philosophical Magazine*, 41:744–746.

Villarreal, A. and Asada, H. (1991). A geometric representation of distributed compliance for the assembly of flexible parts. In *International Conference on Robotics and Automation*.

Xia, Y., Yin, Y., and Chen, Z. (2006). Dynamic analysis for peg-in-hole assembly with contact deformation. *International Journal of Advanced Manufacturing Technologies*, 30:118–128.